Proceedings of the Project Review, Geo-Mathematical Imaging Group (Purdue University, West Lafayette IN), Vol. 1 (2009) pp. 193-204.

SEISMIC WAVE PROPAGATION ACROSS IN-FILLED FRACTURES

ANGEL A. ACOSTA-COLON*, MICHAEL K. OLANDER†, AND LAURA J. PYRAK-NOLTE‡

Abstract. Natural fractures are often filled with debris that form a sub-porosity within the fracture void space. In this study, we investigate the effect of a sub-porosity on seismic wave propagation across a fracture and consequently our ability to probe changes in the fractures properties caused by the formation or alteration of a sub-porosity. Laboratory experiments were performed to examine acoustic wave scattering from layers of spherical beads that constitute a sub-porosity within a synthetic fracture. Compressional waves were transmitted across the fracture using contact piezoelectric transducer. The analysis of the seismic response was performed for a fixed aperture with different sub-porosity created by single and multiple layers of spherical beads. The analysis consisted of wavelet transformation of the seismic signals. Interpretation of the acoustic response depends critically on understanding the length scales associated with the layers (bead diameter, layer thickness), the aperture of the fracture and seismic length scales (wavelengths, field of view). The detection of multiple layers of debris within a fracture is possible by understanding wave interference, dispersion and the reflections in the waveform.

1. Introduction. Fractures and joints in the field often contain debris or rubble between the walls of these mechanical discontinuities. These debris originate from many different mechanisms: organic and/or inorganic chemical reactions (such as mineralization or biomineralization), sediment transport, formation of the discontinuity (rupture, shearing, etc.), mechanical weathering or combinations of these processes. In many cases, the presence of debris forms a sub-porosity within the void spaces of a fracture. The material that composes this sub-porosity can differ or be the same in chemical and physical properties as that from the fracture walls. The sub-porosity may partially fill voids, thereby reducing the local porosity to length scales on the order of sub-microns to tens of microns. A sub-porosity can reduce or enhance the fracture porosity, permeability and storativity by either filling in the fracture void space or propping the fracture open.

Several laboratory studies have measured the acoustic properties of spherical beads in fluids. Most of these measurements are obtained using seismic reflection methods [5] to simulate marine field measurements. Other experiments consisted of simulating sediment transport where the spherical beads are submerged in a fluid and free to move [3, 4]. These and other studies have shown that beads produce acoustic scattering signatures that depend on the relative size of the bead to the wavelength, λ, of the acoustic signal. The size of the bead/scatterer, a, and the wave number, k ($k = 2\pi/\lambda$) of the signal determines the frequency-dependent nature of the attenuation response. For Rayleigh scattering ($ka < 1$), the attenuation coefficient is proportional to the fourth power of frequency. For resonance (Mie) scattering, the attenuation coefficient depends on the first power of frequency when the wavelength approaches the size of the scatterer. Mie scattering is commonly observed in monodispersions of glass beads in fluidized beds [3].

Characterization of the mechanical, seismic and hydraulic properties of fractures is affected by the geometry of the grains or particles that compose the sub-porosity filling a fracture or mechanical discontinuity. In nature, the size of the material that in-fills or creates a sub-porosity inside a fracture or other mechanical discontinuity varies depending on the geologic setting. Mechanical discontinuities (joints, pipes, caves, faults, etc.) and the infill material can vary in size from microns to millimeters to meters. For example, in a tunnel on the Runcorn Peninsula, UK [12] infilled fractures with apertures as large as 35 mm were found to be filled with fine to medium grain sands (0.125 - 0.5 mm). A field study of sediment fissures in soils in the Chihuahuan Desert of Texas, USA observed apertures that ranged from 25 mm to 65 mm with sediment infill that ranged from clay-size particles to clast-supported gravel, a size range of approximately 5 microns to 10 mm [11]. From a study of ancient karst environments [6], mechanical discontinuities, such as fractures, pipes

*Earth and Atmospheric Sciences Department, Purdue University, West Lafayette, IN 47907

†Department of Physics, Purdue University, West Lafayette, IN 47907, Department of Earth and Atmospheric Sciences, Purdue University, West Lafayette, IN 47907

‡Department of Physics, Purdue University, West Lafayette, IN 47907, Department of Earth and Atmospheric Sciences, Purdue University, West Lafayette, IN 47907

and caves, ranged in size from a few millimeters to several meters and were often filled with sediment that range from clays (a few microns) to boulders ($\sim$ meter).

Thus, in addition to the length scales associated with fracture geometry (aperture, surface roughness, contact area distributions, spatial correlation lengths), the length scales associated with the infilling material must also be considered relative to the wavelength of the signal as well as the scale of the region probed [1]. The interpretation of the seismic measurements will be affected by scattering from the fracture and potentially by scattering from the infill material.

In this study, we used a synthetic fracture to investigate the effect of different sub-porosities (grain size, layer thickness and number of layers) on the wave propagation across an infilled fracture.

2. Experimental Method and Data Analysis. Laboratory seismic measurements were performed to investigate the effect of a sub-porosity on wave propagation across an open fluid-filled fracture. The experiments were performed to examine seismic wave scattering from layers of acrylic (Lucite) beads that were used to create a sub-porosity within a synthetic fracture. The experimental setup consisted of a synthetic fracture created by the separation of two acrylic right-cylinders (Figure 1). The thicknesses of the cylinders were 25.4 mm (top cylinder) and 35 mm (bottom cylinder). The bottom cylinder contained an 18 mm deep recess, which was filled with water and the sub-porosity. The aperture of the fracture was controlled by using a computer-controlled linear actuator to increment the aperture from contact (0 mm) to 20 mm in increments of 50 microns.

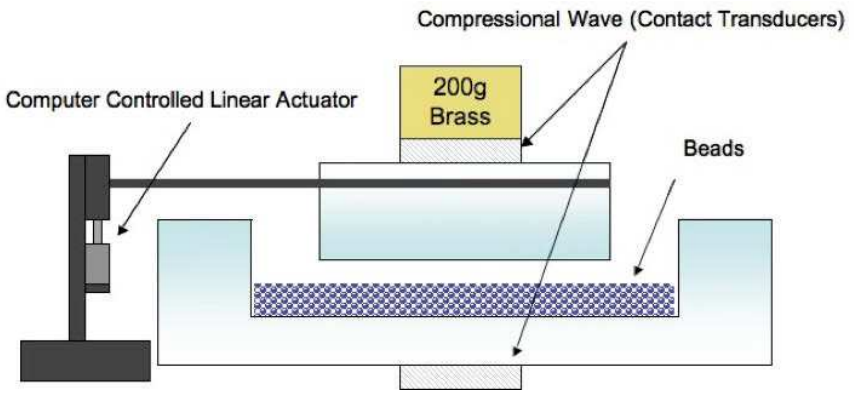

FIG. 1. *Experimental set up to measure the effects of the sub-porosity on the wave propagation across a fracture. The top and bottom acrylic cylinders create the fracture.*

Sub-porosities were created to examine the effect of grain size, number of layers and mixtures of grain sizes on seismic wave propagation. The sub-porosity in the fracture was created by using spherical beads. The specific grain sizes and number of layers are given in Table 2.1. The synthetic fracture was saturated with water and the sub-porosity (layers of beads) was packed in the bottom cylinder. The effect of grain size on wave propagation across an in-filled fracture was studied by using a single layer of beads with a uniform size. Four single layer experiments were performed using bead sizes of $0.5\lambda_L$, λ_L, $2\lambda_L$, and $3\lambda_L$, where λ_L is the wavelength in acrylic and is approximately 2.37 mm for a frequency of 1 MHz. The effect of successive deposition of a uniform bead size was investigated by measuring the response of a single layer to several layers (2 to 6 layers) all composed of the same bead size ($0.5\lambda_L$). Finally, the seismic response of a mixture of bi-modal grain sizes ($0.5\lambda_L$, & $3\lambda_L$) was measured for infill with the same quantity of each size bead but with different substructures to determine if the different substructures can be seismically delineated.

Compressional waves were transmitted across the fracture using contact piezoelectric transducers (central frequency of 1 MHz) for both the source and receiver transducers. The contact transducers were not removed from the sample between experiments to reduce error associated with the repeatability of coupling of the transducers to the sample. A 200 gram mass was placed on top

TABLE 2.1
Spherical beads diameters used in the sub-porosity experiments and its equivalent as a function of the signal wavelength for its material (Lucite).

Experiment	**Bead Size (mm)**	**WaveLength Size $\lambda_L = 2.72$ mm**
Successive Deposition - Lucite		
1 layer	1.47	$0.5\lambda_L$
2 layers	2.67	λ_L
3 layers	3.87	$1.4\lambda_L$
4 layers	5.07	$1.85\lambda_L$
5 layers	6.27	$2.27\lambda_L$
6 layers	7.47	$2.72\lambda_L$
Grain Size - Lucite		
1 layer	1.47	$0.5\lambda_L$
1 layer	3.05	λ_L
1 layer	5.41	$2\lambda_L$
1 layer	7.79	$3\lambda_L$
Mixture - Lucite	7.79 & 1.47	$3\lambda_L$ & $0.5\lambda_L$

of the transducer to prevent movement of the transducer during measurements.

Seismic measurements were made as a function of aperture. The contact aperture (relative to the source to receiver configuration) varied depending on the size of the grain and number layers in the fracture for a given experiment (e.g., one layer had a smaller contact aperture than a multi-layer experiment). To eliminate seismic effects due to the fracture aperture, the analysis was performed on data from each experiment collected at a constant aperture of 7.79 mm for the successive deposition and grain size analysis. For the mixture of bead sizes experiments, the contact aperture was used for analysis (approximated 9.36 mm).

3. Analysis. Compressional waves were used to investigated the effect of a sub-porosity on wave propagation across a fracture. Data analysis on the measured signals included a time-frequency analysis [10] to obtain dispersion and wave interference from the first arriving compressional wave (P-wave). The time-frequency analysis (wavelet transform) provides the variation in frequency content of the signal as a function of arrival time. The spectrum from the wavelet analysis at the arrival time of the dominant energy was used to examine the variation in effective fracture stiffness using the displacement discontinuity theory [2, 7, 9]. A transmission coefficient, $T(\omega)$, was calculated by taking the ratio of the spectrum from the fracture with a sub-porosity to that from the water-filled fracture with the same aperture. $T(\omega)$ was used to calculate an effective fracture stiffness for the fracture containing a sub-porosity. Using equation 3.1, an effective fracture stiffness, k, is calculated as a function of frequency, ω, for a known acoustic impedance of acrylic, Z (phase velocity*density).

$$k(\omega) = \frac{\omega Z}{2\sqrt{\left(\frac{1}{T(\omega)}\right)^2 - 1}} \tag{3.1}$$

In our analysis, we used a phase velocity of 2730 m/s and a density of 1180 kg/m^3 for the acrylic, i.e., an acoustic impedance of 3.22 x 10^6 kg/m^{2}s. The calculated stiffness is an effective stiffness because the fracture aperture and asperity spacing are much greater than a wavelength, which is the limit of validity of the displacement discontinuity theory. However, in our study, the use of broadband transducers enables us to examine both the short-wavelength and long wavelength regime, i.e. the results span the limits of the theory. The variation in effective fracture stiffness with

frequency is used to determine when the fracture is in or deviates from displacement discontinuity like behavior versus short-wavelength behavior.

4. Results and Discussion.

4.1. Successive deposition of same grain size. Sub-porosities consisting of single and multiple layers composed of acrylic spheres 1.47 mm in diameter ($0.5\lambda_L$) were used to simulate successive deposition of the same grain size with the same material properties as the fracture walls. The transmitted compressional waves for the different fracture fillings are shown in Figure 2 for a fixed aperture of 7.79 mm. Relative to water, as the number of layers (successive deposition) in the fracture increases, the velocity of the compressional wave increases and the interference among phases results in a decrease in the period (or increase in the frequency). The velocity increases because the compressional wave velocity in the Lucite bead (2730 m/s) is faster than in water (1480 m/s). In Figure 3, the results of the time-frequency analysis for signals from the water-filled fracture and the in-filled fractures (Figure 2) are shown. A wavelet analysis of the signals is shown in Figure 3 was performed to examine the change in frequency content with increasing number of layers of grains as well as to determine signatures of interference. The time-frequency response of the water-filled fracture is used to examine the effect of a fluid-filled fracture aperture (7.79 mm) on the dispersion and spectrum. The water-filled fracture signal is essentially non-dispersive (i.e., the velocity does not significantly depend on frequency) and the dominant energy occurs at a frequency of $\sim$ 0.78 MHz. When one layer of beads partially fills the fracture, the wavelet exhibits more energy at low frequencies (0.2 - 0.3 MHz) and a slight shift in the dominant frequency (0.8 MHz). As more and more layers fill in the fixed aperture fracture, an interference null or stop-band is observed between 0.35 MHz and 0.5 MHz, and more energy is observed in the low frequency components of the signal relative to the high frequency components.

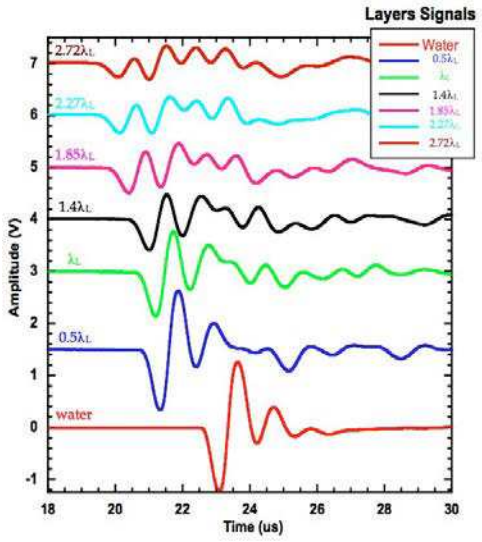

FIG. 2. *Layering effect in the first arrival of the seismic response of the fractures with water (red) a single layer of R0.5 (blue) and multiple layers (2 layers = green, 3 layers = black and 4 layers = pink, 5 layers = cyan and 6 layers = cayenne).*

From the wavelets, spectra were extracted from the wavelet at the time where the dominant frequency arrives (Figure 4a). A notch or a stop band is observed in the frequency spectra as soon as two layers of bead partially fill the fracture. The frequency at which the stop-band occurs and the width of the stop band is used to calculate the bead size and the impedance contrast of the infill material, respectively [13]. From interpretation of the stop-band, the bead size was calculated to be 1.35 mm (actual value 1.47 mm) based on the notch frequency (0.35-0.5 MHz). The impedance

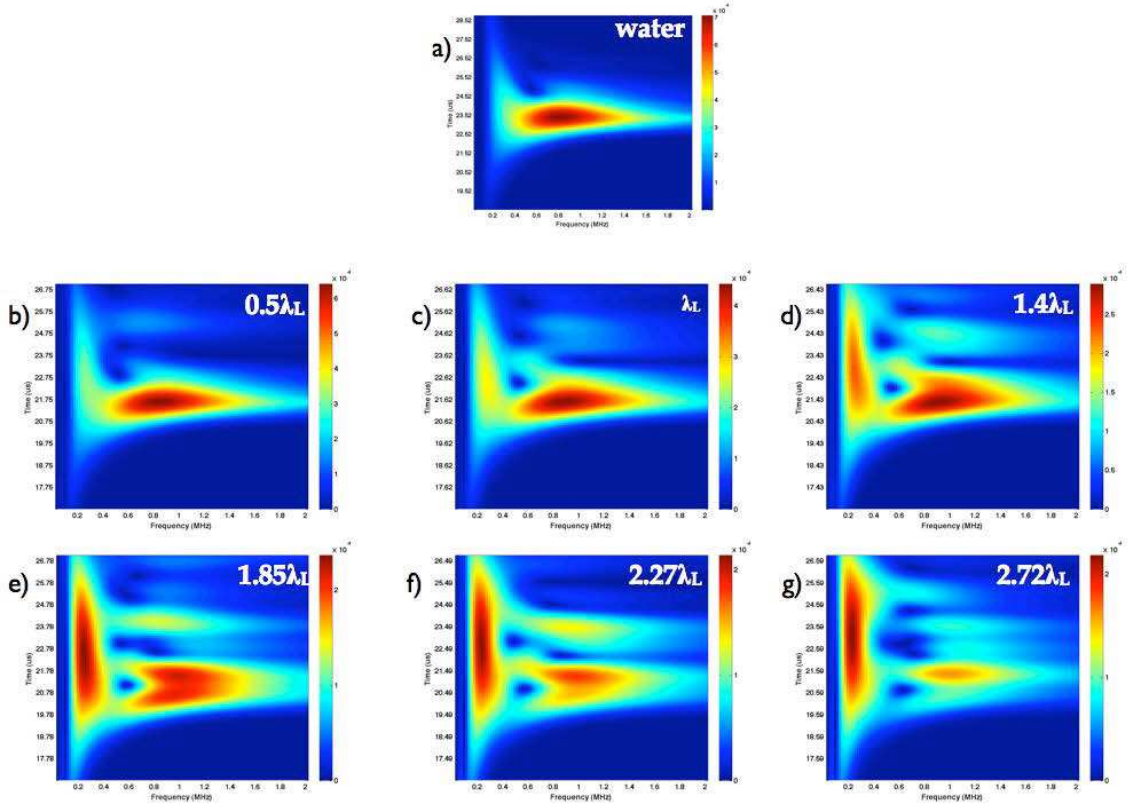

FIG. 3. *Wavelet transformations for the multiple layers signals. The interference null is observed for the wavelets (dark blue region), a) single layer of R0.5 and multiple layers: b) 2 layers, c) 3 layers, d) 4 layers, e) 5 layers and f) 6 layers.*

contrast (between water and acrylic) calculated from the width of the stop band was calculated to be 1.34 (actual value 1.29).

The stop-band spectrum is essentially a notch filter and is affected by the size of the bead size and the wavelength of the signal. In our experiments, multiple layers created a notch filter that affected the spectra of the signals. We used the compressional wave signal from the water-filled fracture and a notched frequency filter (i.e., spectrum from 4 layer case) to try to reproduce the waveform from the 4 layer experiment. Figure 4b shows the result of a theoretical analysis to simulate the seismic response of 4 layer case with a notch filter and the signal from the water-filled fracture. As is shown in Figure 4b, the filtered signal is similar to the signal with the infill in phase except for the first arrival. Observations of stop band behavior provide a method for determining the properties of infill material in a fracture or other mechanical discontinuity.

4.2. Grain size. Experiments were performed to study the effects of increasing grain size of a single infill layer on wave propagation across a fracture. The transmitted compressional waves from the water filled fracture and the fracture filled with a single layer of beads of size $0.5\lambda_L$, λ_L, $2\lambda_L$, and $3\lambda_L$, are shown in Figure 5. By inspection of the signals, the velocity increase as grain size increases and the low frequency components of the signal arrive earlier for larger grain sizes. The compressional wave is observed to be composed of a combination of a wave propagated through water and through the bead layer. When the grain size is greater than a wavelength ($2\lambda_L$ and $3\lambda_L$), the first arrival (or prompt wave around 19 μs) is attenuated and contains low frequency as observed from the period of this mode. This prompt wave is the portion of the wave that traveled mainly through the beads that have a compressional wave velocity that is faster than that of water. The

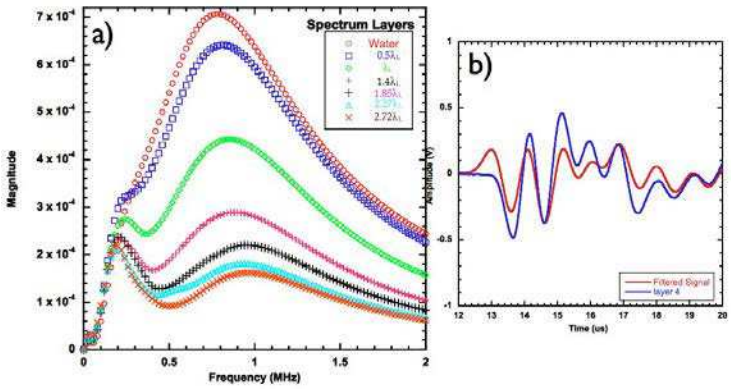

FIG. 4. *(a) Frequency spectrum extracted from the wavelets for the seismic response for the multiple layers experiments, the spectrum was extracted from the time at the dominant frequency of the signal arrives. (b) Theoretical calculation of the effects of the notch in the seismic response. The frequency spectrum of the water signal is multiplied by a frequency spectrum with a notch and the signal is inversely obtained, then the filtered signal (red) is compared to the 4 layer seismic signal (blue) that have a similar frequency notch.*

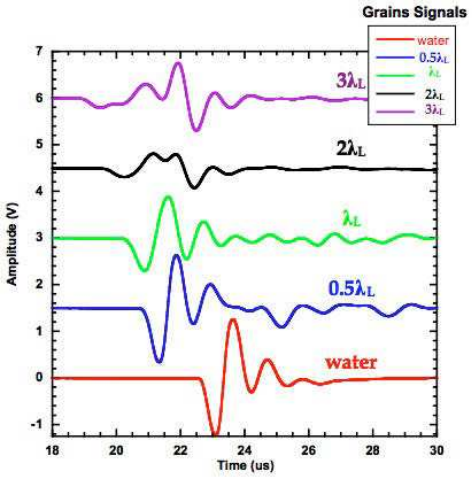

FIG. 5. *Grain size effect in the first arrival of the seismic response of the fractures filled with a single layer of* $0.5\lambda_L$ *(blue),* λ_L *(green),* $2\lambda_L$ *(black),* $3\lambda_L$ *(violet) and water (red).*

main energy (large amplitude portion of the signal) of the signals for grain sizes larger than λ_L is the portion of the wave that traveled mainly in water (around 22 μs). In contrast, for a grain sizes less than the λ_L, the signature of the single layer of beads is given by the "shoulder wave". This shoulder wave is an interference wave arriving later than the main energy (around 22.5 μs) for a grain size $0.5\lambda_L$ in Figure 5. When the grain size is comparable to λ_L, the interference waves are superimposed and neither the prompt wave nor the shoulder wave are observed.

The group wavelets transformations for the signals shown in Figure 5 are presented in Figure 6. An interference null that occurs from interference between the portion of the wavefront traveling in the water and that traveling mainly through the beads is observed in the wavelets. The interference null associated with the shoulder wave created by the grain size $0.5\lambda_L$ is observed to arrive after the dominant energy at $\sim$ 22.76 μs for a frequency off 0.5 MHz. As the grain size increases, the interference null arrives earlier shifting from 22.75 μs for $0.5\lambda_L$ signal as compared to 21.5 μs for the $3\lambda_L$ signal. For a grain size of $3\lambda_L$, the interference null arrives prior to the dominant energy. The interference null travels from a late arrival time (shoulder wave) to an early arrival time (prompt

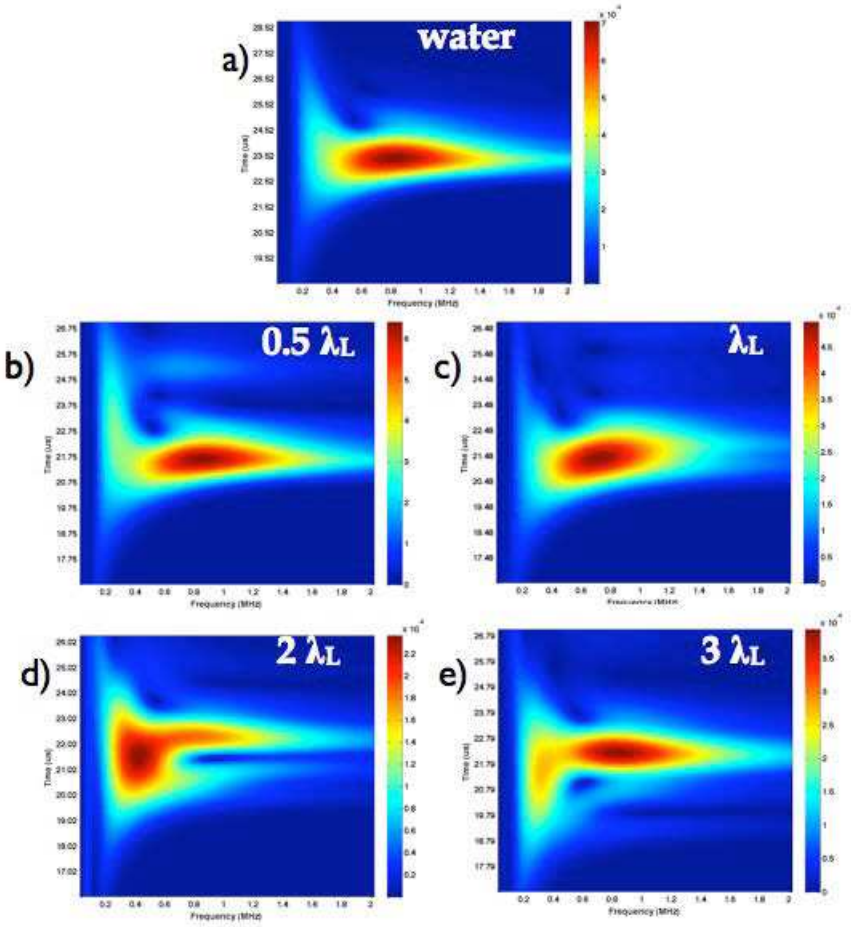

FIG. 6. *Time-frequency analysis (wavelets) results for the first arrival of the seismic signal of the fracture filled with a) water, and single layers of b)* $0.5\lambda_L$*, c)* λ_L*, d)* $2\lambda_L$ *and e)* $0.5\lambda_L$*.*

wave) when the grain size increases.

In addition, the signals are dispersive. The time dispersion curves for the signals were extracted from the wavelets and are shown in Figure 7. The signal from the water-filled fracture (open circles in Figure 7) exhibits very little dispersion between 0.7 MHz and 2 MHz, while below 0.4 MHz, low frequencies are observed to have a late arrival time. For $0.5\lambda_L$ and λ_L grain sizes, the low frequencies component of the transmitted signal arrives later than the higher frequencies component. The slope of the dispersion curves increases with increasing grain size and the frequency at which the signal becomes non-dispersive is also affected by grain size.

An effective stiffness was calculated from the transmission spectrum obtained from the wavelets by using the displacement discontinuity theory (Equation 3.1). The effective stiffness - frequency relationship provides insight on the scattering regime of the infill material. The variation in effective fracture stiffness with frequency is used to classify the seismic response of a fracture containing a sub-porosity. A linear dependence on frequency of effective fracture stiffness occurs when a layer behaves as a welded contact or is in the geometric ray regime. A frequency-independent effective stiffness occurs when the layer behaves as a non-welded contact (displacement discontinuity) with a uniform effective stiffness [8]. Figure 8 shows the effective stiffness from the single layer experiments with different grain sizes. From the effective stiffness vs. frequency relationship, we observed that only the λ_L case behaves as a uniform non-welded contact (i.e., stiffness is independent of frequency)

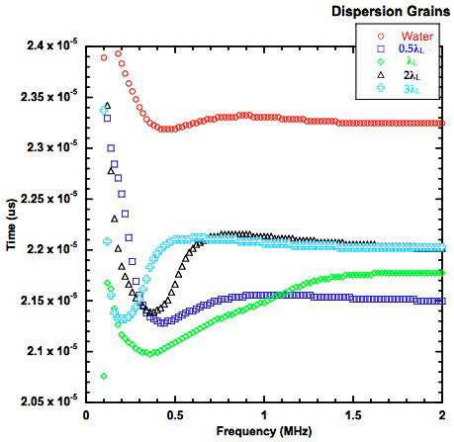

FIG. 7. *Dispersion extracted from the wavelets for the grain size seismic response of the fractures with water (red circle) a single layer of* $0.5\lambda_L$ *(blue squares),* λ_L *(green diamonds),* $2\lambda_L$ *(black triangles) and* $3\lambda_L$ *(cyan crosses).*

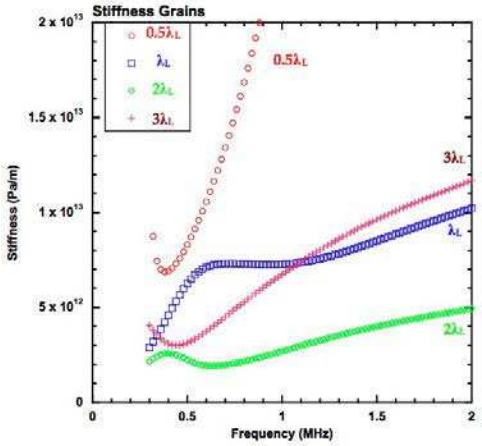

FIG. 8. *Fracture effective stiffness obtained from the frequency spectrum of the seismic measurements for the water saturated fracture with different grain size, a single layer of* $0.5\lambda_L$ *(red circles),* λ_L *(blue squares),* $2\lambda_L$ *(green diamonds) and* $3\lambda_L$ *(cayenne crosses).*

for frequencies between 0.5 MHz – 1.0 MHz, or roughly for wavelengths greater than or equal to the contact spacing (diameter of the grain). The linear dependence of effective stiffness with frequency for $2\lambda_L$ and $3\lambda_L$ indicate behavior in the geometric or ray regime. For 0.5λ, the effective stiffness rapidly diverges as frequency is reduced, indicating Rayleigh regime behavior. The effective specific stiffness enables interpretation of infill material size based on the scattering behavior of the waves.

4.3. Comparison of Sub-porosity Substructure with Similar sizes. A goal of this study was to determine if the structure of the sub-porosity could be delineated for two sub-porosities that are similar in height but differ in substructure. The signal from a single layer of large beads was compared to the signal from several layers of small beads but with a thickness equivalent to that of the single layer. As observed in the data in the previous section, the seismic response to a sub-porosity within a fracture is controlled by the bead size and number of layers. We present two examples of similar size, the single bead layer of λ_L (bead size is 3.05 mm) compared to 2 layers of $0.5\lambda_L$ (layer height of 2.67 mm), and a single layer of $2\lambda_L$ (bead size is 5.41 mm) compared to 4 layers of $0.5\lambda_L$ (layer height of 5.07 mm). Figure 9a gives the comparison between λ_L and 2 layers of $0.5\lambda_L$, while Figure 9b shows the comparison between $2\lambda_L$ and 4 layers of $0.5\lambda_L$. Inspection

of the first arrival of the seismic measurements shows that the arrival times, phase and frequency content of the signals of single layer and an equivalent layer composed of several layers of smaller beads are different. For both comparisons, the signals from the 2 & 4 layer waveforms arrive later than the signal from the single layer, and exhibit more interference.

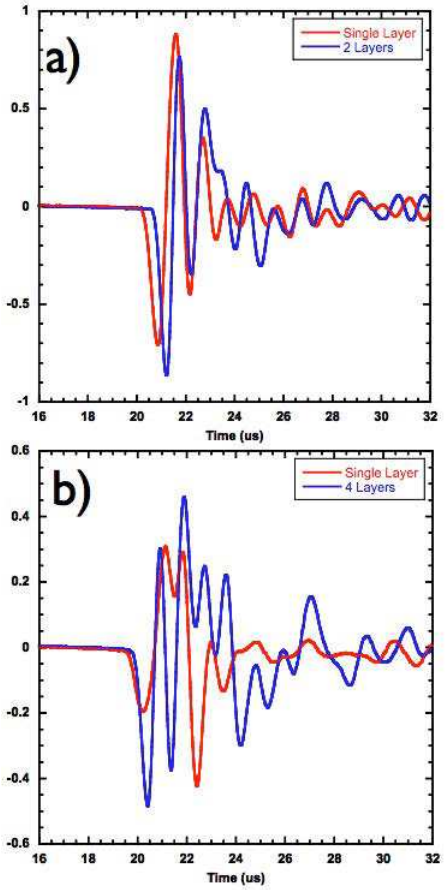

FIG. 9. *Comparison of the signals for the fracture filled with single bead (red) and equivalent size composed of multiple layers (blue).*

The wavelets of the signals were presented earlier in this paper. The wavelets of the single layer of 3.05 mm and the single layer of 5.41 mm are shown in Figure 6c and 6d respectively. For the multiple layers wavelets, the transforms for the 2 layer and 4 layer measurements are shown in Figure 3c and 3e, respectively. From a comparison of the wavelets, the interference nulls are observed in the wavelets for the multiple layer cases (2 & 4 layers) indicating strong interference. For the multiple layers, the low frequencies arrives later than from the single layer. The dispersion curves for an equivalent layer sample and a single layer sample are also very different especially for the 5.41 mm bead size and equivalent layer of 5.07 mm. The single layer of beads exhibits increasing arrival time with increasing frequency while the equivalent layer exhibits a decreasing arrival time with increasing frequency.

Substructure of the sub-porosity affects the seismic response of the fracture because the scattering response depends on the size of the grain relative to a wavelength as well as the spacing between of layers relative to the wavelength. For example, the stop-band behavior observed for the 4 layer measurements composed of grains of 1.47 mm occurs when the bead spacing is approximately a quarter of a wavelength, i.e. approximately a frequency of 0.5 MHz. This stop band behavior is not

observed for a single layer of equivalent size.

4.4. Mixture of beads. The effect of a mixture of beads on wave propagation across an infilled fractured was also investigated. A combination of $3\lambda_L$ and $0.5\lambda_L$ beads was used. For each experiment, a different sub-porosity structure was constructed from the same quantity of each bead size (same density in the infill). The different structures were: (a) single layer of $3\lambda_L$ on top of a single layer of $0.5\lambda_L$ (Layers); (b) the previous structure was stirred and allowed to settle (Mixture); and (c) the top voids of a single layer of $3\lambda_L$ were filled with beads of $0.5\lambda_L$, (Voids). The transmitted compressional waves for these three different structures are shown in Figure 10a. Inspecting the compressional wave signals for the three cases, it is observed that they have similar arrival times but different phases, which indicate that the infill material density is the same but the structure is not. The group wavelet transformations for these three datasets are shown in Figure 10b. The frequency of the dominant energy and the energy partitioning among the low and high frequencies component of the signal are affected by the substructure. The differences in energy partitioning occur because each structure had a different water-bead path resulting in different scattering mechanisms. For example, the wavefront in the Layer case exhibits less scattering because the wave initially interacts with the $3\lambda_L$ layer compared to the Mixture case where the wave firsts interacts with a mixture of the two grain sizes. The structure attenuates the high energy components because of scattering created by the initial interaction of the wavefront with the infill material. Analysis of the scattering due to the structure provides a method for determining heterogeneity in the infill of fractures.

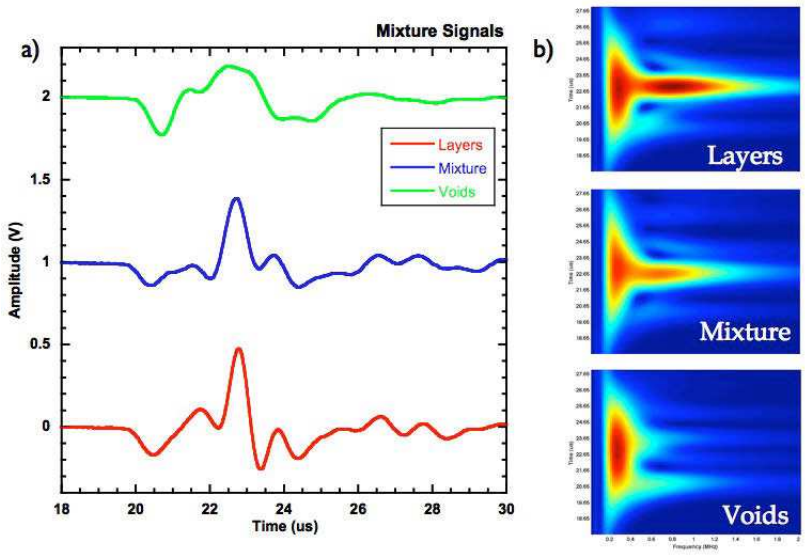

FIG. 10. *(a) Seismic response of the different cases of the mixture of beads and (b) the wavelets from first arrival of the seismic signals of the mixture cases.*

5. Summary. The ability to distinguish a sediment-filled or partially sediment-filled fracture from a water-saturated fracture depends on the size of the sediment grains relative to a wavelength. We observed that dispersion, interference nulls and seismic velocities were the prime indicators of the presence of a sub-porosity created by grains (beads) within a fracture. For successive deposition of same grains, the layering resulted in observation of stop band (frequency notch) behavior that provides information on the grain size, impedance contrast and potentially the number of layers. From the experiments on single layers but with different grain sizes, the signature of the infilled material is related to the scattering regime and the relationship between the grain size and the signal wavelength. The scattering regime can be determined by characterizing the fracture with an effective stiffness. From the experiments with a mixture of grain sizes, the structure of the grains

significantly affects the frequency content of the signal.

In conclusion, the detection of multiple layers of debris within a fracture or other mechanical discontinuity is possible by understanding wave interference, dispersion and scattering signatures in the waveforms. The length scales of the infill material (sub-porosity) in a fracture affect seismic wave propagation. The length scales include the size of the grains, the number of layers, layer thickness, the structure and the seismic scales (i.e wavelength and field of view) as well.

REFERENCES

[1] A. A. Acosta-Colon, L. J. Pyrak-Nolte, and D. D. Nolte. Laboratory-scale study of field-of-view and the seismic interpretation of fracture specific stiffness. *Submitted and accepted to Geophysical Prospecting*, 2008.

[2] Gu B.L., K.T. Nihei, L.R. Myer, and L.J. Pyrak-Nolte. Fracture interface waves. *Journal of Geophysical Research-Solid Earth*, 101:827–835, 1996.

[3] M.L. Cowan, K. Beaty, J.H. Page, Z. Liu, and P. Sheng. Group velocity of acoustic waves in strongly scattering media: Dependence on the volume fraction of scatters. *Physical Review E*, 58:6626–6636, 1998.

[4] Y. Le Gonidec and D. Gilbert. The wavelet response as a multiscale characterization of scattering processes at granular interfaces. *Ultrasonics*, 44:381–390, 2006.

[5] Y. Le Gonidec, D. Gilbert, and J. Proust. Multiscale analysis of waves reflected by complex interfaces: Basic principles and experiments. *Journal of Geophysical Research*, 107:2184–2199, 2002.

[6] E. Juhasz, L. Korpas, and A. Balog. Two hundred million years of karst history, dachstein limestone, hungary. *Sedimentology*, 42:473–489, 1995.

[7] Pyrak-Nolte L.J., L.R. Myer, and N.G.W. Cook. Transmission of seismic-waves across single natural fractures. *Journal of Geophysical Research-Solid Earth and Planets*, 95:8617–8638, 1990.

[8] Pyrak-Nolte L.J. and D.D. Nolte. Frequency-dependence of fracture stiffness. *Geophysical Research Letters*, 19:325–328, 1992.

[9] Schoenberg M. Elastic wave behavior across linear slip interfaces. *Journal of the Acoustical Society of America*, 5:1516–1521, 1980.

[10] D. D. Nolte, L. J. Pyrak-Nolte, J. Beachy, and C. Ziegler. Transition from the displacement discontinuity limit to the resonant scattering regime for fracture interface waves. *International Journal of Rock Mechanics and Mining Sciences*, 37:219–230, 2000.

[11] B. R. Scanlon. Moisture and solute flux along preferred pathways characterized by fissured sediments in deserts soils. *Journal of Contaminant Hydrology*, 10:19–46, 1992.

[12] G. P. Wealthall, A. Steel, J.P. Bloomfield, R.H. Moss, and D. N. Lerner. Sediment filled fractures in the permo-triassic sandstones of the cheshire basin: observations and implications for pollutant transport. *Journal of Contaminant Hydrology*, 50:41–51, 2001.

[13] A Yariv. *Optical Waves in Crystals: Propagation and Control of Laser Radiation*. Wiley-Interscience, 1983.